PCCP

Accepted Manuscript

ROYAL SOCIETY OF CHEMISTRY

www.rsc.org/pccp

Physical Chemistry Chemical Physics
CREATED USING THE RSC LaTeX PCCP ARTICLE TEMPLATE – SEE www.rsc.org/electronicfiles FOR DETAILS
ARTICLE TYPE www. rsc.org/xxxxxx | XXXXXXXX

Performance analysis of energy conversion via caloric effects in first-order ferroic phase transformations

Yintao Song[a]

Received Xth XXXXXXXXX 20XX, Accepted Xth XXXXXXXX 20XX
First published on the web Xth XXXXXXXXX 200X
DOI: 10.1039/b000000x

A finite-time thermodynamic model of ferroic refrigerators and generators, based on first order phase transformation, is given. We use this model to evaluate a novel method of converting heat directly into electricity based on the martensitic phase transformation accompanied by an abrupt change in magnetic ordering recently discovered [Srivastava *et al.*, *Adv. Energy Mater.*, 2011, **1**, 97]. In this paper, we study the efficiency and power output of this method. The formulas of efficiency and power output in terms of material constants, design parameters, and working conditions are derived. The Clausius-Clapeyron coefficient is shown to be important to the efficiency. The figure of merit, as a dimensionless parameter, of energy conversion using the new method is introduced. It is shown that, as the figure of merit goes to infinity, the efficiency approaches the Carnot efficiency. Thermodynamic cycles of the new energy conversion method are optimized for a maximum power output. The matching criteria between materials and working temperatures of such optimized cycles are derived. Using these criteria, one can choose the most suitable materials at given working conditions, or decide the best working conditions for available materials.

1 Introduction

Materials that can change their ferroic properties, such as ferromagnetism, ferroelectricity and ferroelasticity, as changing the temperature are often used to convert energy between heat and other forms, *e.g.* magnetostatic, electrostatic and elastostatic energy. The usage of this effect, in the ferromagnetic regime, in refrigeration and electricity generation was demonstrated by Warburg[1] and Tesla[2] (among others) already in 1800's. Their works have latter been named *magnetocaloric effect* and *pyromagnetic generators*, respectively. Later, the analogous concepts for ferroelectricity, *i.e. electrocaloric effect*[3–5] and *pyroelectric generators*[6–8], emerged too. The thrust of ferroic energy conversion for eco-friendly refrigeration applications was the discovery of the so-called *giant* magneto- and electrocaloric effects[9,10]. Also, a novel method of electricity generation using giant magnetocaloric materials has been demonstrated by Srivastava *et. al.*[11]. Examples of reviews on this class of materials are Refs. 5,12–16. These giant ferroic-caloric effects originate in first order phase transformations, where the ferroic properties and the entropy exhibit discontinuous jumps[17,18]. These first order phase transformations are generally martensitic (diffusionless, displacive) phase transformations, during which the intrinsic ferroic property having a discontinuous jump is the ferroelastic strain. Inspired by this fact, the concept of (giant) elastocaloric refrigerators[19] and ferroelastic (shape memory) generators[20] has also been proposed and demonstrated.

In a nutshell, during a multiferroic martensitic phase transformation, the material exchanges heat with the environment through the entropy change, and exchanges magnetostatic, electrostatic or elastostatic energy through the jumps of ferromagnetic, ferroelectric or ferroelastic properties. The interplay among these energy flows results in applications of refrigeration and electricity generation. The purpose of this paper is to develop a thermodynamic model to evaluate the performance of these energy conversion mechanisms, and the implication on materials development and devices design for future improvements. Since the thermodynamic analysis of heat engines and refrigerators are almost completely analogous, we focus on the former and assume that the extension to the latter is easy. In particular, we are going to study the efficiency and power output of the new electricity generation method demonstrated by Srivastava *et al.*[11].

Thermodynamic theories of ferroic-caloric materials aim at predicting energy conversion performance using the data from the two major classes of characterization techniques of ferroic-caloric materials: *direct* and *indirect* measurements. In a direct measurement, through precise calorimetry, the materials response $\theta(F)$ is measured, from which the quantity $\Delta\theta/\Delta F$ is obtained, where θ is the temperature and F is the thermodynamic conjugate variable (driving force) of the ferroic property, denoted X in this paper. For example, F is the magnetic inductance if X is the magnetization. Since

precise measurement of heat absorption and release is difficult in practice, an easier indirect method has also been widely used. This method measures the material response as a function $X(F,\theta)$. The underlying thermodynamic argument is the Maxwell relation $\partial X(F,\theta)/\partial\theta = \partial S(F,\theta)/\partial F$, where S is the entropy. Due to this consideration of experimental simplicity, this work, following our previous paper[21], is based on the thermodynamic function $X(F,\theta)$ and the resulting Gibbs free energy $G(F,\theta)$ which can be fitted[21] by indirect measurement data.

Since most of the existing thermodynamic models[6,7,21,22] of ferroic-caloric energy conversion are quasi-static in nature, they cannot predict the power output. An consideration of rate-dependence of the thermodynamic processes of the system is necessary. The simplest rather acceptably accurate finite-time thermodynamics is the *endoreversible thermodynamics* proposed by Curzon and Ahlborn[23] (see also Ref. 24–28). The terminology "endoreversibility", as proposed by Rubin[26], means that the irreversibility only comes from the heat exchange between the working material and heat reservoirs, while the working material internally still performs reversible processes. The losses due to the finite rate of processes are located only in the interaction between the reversible subsystem and its environment. Van den Broeck *et al.*[29] proved that the efficiency formula derived by Curzon and Ahlborn[23] (the C-A efficiency) agrees with, without approximation, the theory of linear irreversible thermodynamics, universally up to the quadratic order in the deviation from equilibrium[30]. In this paper, we adopt the assumption of endoreversibility to establish a finite-rate thermodynamic model that is capable of predicting the power output of the new energy conversion method (Sect. 2 and 2.3). Analytic formulas of rate-dependent efficiency and power output will be derived. A natural application of endoreversible thermodynamics is the prediction of cycles with maximum power output[31,32]. We study ferroic-caloric energy conversion cycles working at maximum power output (Sect. 2.3), with two possible heat transfer mechanisms: i) convective heat exchange modeled by the Newton's law of cooling, like what Curzon and Ahlborn[23] did, and ii) radiative heating modeled by a constant heating power supply. By applying the results to the example of ferromagnetic-ferroelastic materials (Sect. 3), we are able to identify the essential parameters influencing the efficiency and power output, such as the coefficient in the Clausius-Clapeyron relation and the *figure of merit*. The dependence of the figure of merit on the shape of the specimen is explored in Sect. 3.3.

A further question naturally arises here: which material has the correct properties to perform the optimized (maximum power output) cycle predicted for given working conditions? The key to the answer is the constitutive properties, such as heat capacity[33], of the working material. By relating these parameters to the study on cycles working at maximum power, we obtain the matching criteria between the devices (material properties + design parameters) and working temperatures for the best performance. Using these criteria, one can choose the most suitable materials/devices for the target working conditions, as well as decide the best working conditions for the candidate materials/devices on hand. These criteria are discussed in Sect. 3.4.

Before entering the main content of the paper, we want to make a remark about hysteresis of first order (martensitic) phase transformations in ferroic-caloric materials. Hysteresis is a loss of energy due to irreversible processes during phase transformation cycles. It reduces the energy conversion efficiency[34] and causes the functional degradation of materials[35]. Such a loss cannot be avoided by any device design strategy. An effective way of minimizing hysteresis relies on systematic material development. By tuning the compositions of the alloy, the lattice parameters can be made to satisfy the geometrical compatibility condition $\lambda_2 = 1$[36,37], where λ_2 is the middle eigenvalue of the transformation stretch matrix. The idea is that when $\lambda_2 = 1$, the stress field at the austenite/martensite interface caused by lattice misfit is eliminated.[38,39] Experiments, *e.g.* Ref. 35,40,41, have confirmed that this strategy leads to low hysteresis, highly stable martensitic materials. The material used as an example in this paper, the $Ni_{45}Co_5Mn_{40}Sn_{10}$ alloy, has $\lambda_2 = 1.0032$ and a hysteresis as low as 6 °C[17]. Even in materials not satisfying $\lambda_2 = 1$ by its intrinsic lattice parameters, if the twin wall energy is low, they can form self-organized (adaptive) nanoscale twin laminate whose macroscopically average lattice satisfies $\lambda_2 = 1$.[42] This has been confirmed in both ferroelectric[43] and ferromagnetic[44] martensites. Therefore, in the rest part of this paper, we neglect the thermal hysteresis in phase transformations, which is in fact also consistent with the assumption of endoreversibility mentioned above.

2 Thermodynamics of Phase Transformation

The thermodynamics of fully non-equilibrium processes is still a difficult problem nowadays. Often, various assumptions are adopted to study finite-rate processes so that analysis analogues to that used in equilibrium thermodynamics, *e.g.* Gibbs' theory[45], can be used. In this paper, we validate Gibbs' picture of first order phase transformation by adopting the assumption of endoreversibility[23,28]. Hence, we are able to model finite-rate – but not far away from equilibrium – processes for energy conversion using phase-changing multiferroic materials.

2.1 Clausius-Clapeyron relation and thermodynamic cycles

Let the ferroic property of a material is represented by an internal variable X. Examples of X include magnetization and electric polarization. Its thermodynamic working conjugate force is denoted F, *i.e.* the thermodynamic force corresponding to X. Examples of F include magnetic or electric field along the direction of magnetization or electric polarization. Thus, in the cases considered in the current paper, X and F are both non-negative, as they are assigned the same positive direction. One can also think them as the magnitudes of X and F along a common direction. Choosing the material as our thermodynamic system, the Gibbs free energy is then defined by the following two Maxwell relations:

$$\frac{\partial G(F,\theta)}{\partial F} = -X, \quad \frac{\partial G(F,\theta)}{\partial \theta} = -S, \tag{1}$$

where θ and S are temperature and entropy of the material respectively. According to Gibb's theory, a first order phase transformation occurs at the transformation temperature T that satisfies

$$G_{\rm m}(F,T(F)) = G_{\rm a}(F,T(F)), \tag{2}$$

where the subscripts "m" and "a" denote the low and high temperature phases respectively, since we have martensitic phase transformation as the model in mind. Note that, as indicated by Eqn. (2), the transformation temperature depends on the thermodynamic force. In general, we need the explicit forms of $G_{\rm m}$ and $G_{\rm a}$ in order to solve this equation for $T(F)$, which is called the *Clausius-Clapeyron* relation. Its physical interpretation is the effect of the thermodynamic force on transformation temperature. An example of such a relation in the thermal-magnetic phase-transforming alloy NiCoMnSn was given in Ref. 21.

A useful tool of analyzing the performance of an energy conversion system is the temperature-entropy ($T-S$) diagram, which depends on the constitutive properties of the working material. Fig. 1(a) illustrates the typical constitutive properties of a solid-solid phase-transforming material. The fact that forward transformation offsets from the backward one is due to hysteresis. $T_{\rm as}$ (resp. $T_{\rm ms}$) and $T_{\rm af}$ (resp. $T_{\rm mf}$) are called the austenite (resp. martensite) start and finish temperatures. They could be slightly different from the transformation temperature T determined by the Gibbs' theory.

During a full (endoreversible) thermodynamic cycle, all the state variables of the system, such as internal energy (temperature) and entropy, return to their initial values. Thus, its trajectory on the temperature-entropy plane forms a loop. Suppose during a cycle the system (material) changes its internal energy while doing work and absorbing heat at the rate of Q, the first law of thermodynamics gives the efficiency of converting heat into work output, as defined by Carnot[46], and the average power output of one full cycle as

$$\eta = \int_{\mathscr{C}} Q\,dt \Big/ \int_{\mathscr{C}} (Q+|Q|)/2\,dt, \quad \mathscr{P} = -\frac{1}{|\mathscr{C}|}\int_{\mathscr{C}} Q\,dt, \tag{3}$$

where $\mathscr{C} \subset [0,\infty)$ is the time interval of a cycle.

Although the most efficient energy conversion cycles are Carnot cycles, Rankine cycles and Ericsson cycles are in practice more easier to perform[21], especially for phase-transforming work agents. A Rankine cycle consists of two constant force (isobaric) processes and two adiabatic processes, as illustrated by the "red-black-blue-black" loop in Fig. 1(b). Denote the two constant forces F_+ and F_- corresponding to heating and cooling processes, respectively. In the rest of this chapter, subscripts + or − indicates the variables associated with the isobaric heating or cooling respectively. As shown in Fig. 1(b), a Rankine cycle is initiated at the state $(F_+, T_{\rm s+})$ with $T_{\rm s+} = T_{\rm as}(F_+)$. Then the specimen is heated to the temperature $T_{\rm f+}$, while F_+ is fixed. $T_{\rm f+}$ is determined so that the system has the same entropy of its third state $(F_-, T_{\rm s-})$, where $T_{\rm s-} = T_{\rm ms}(F_-)$, so that we can adiabatically move the system to the latter state. The final process is an isobarically cooling at F_- to the temperature $T_{\rm f-}$, where $T_{\rm f-}$ is determined in the same fashion of determining $T_{\rm f+}$. An Ericsson cycle is obtained by replacing the adiabatic processes (black branches in Fig. 1(b)) with the isothermal and isobaric processes (green branches in Fig. 1(b)). Examples of such a Rankine cycle and an Ericsson cycle in the real material $Ni_{44}Co_6Mn_{40}Sn_{10}$ were given in Ref. 21.

2.2 Ideal phase transformation systems

It is helpful to parameterize the Rankine cycle so that analytic formulas of efficiency and power output can be derived. For our purpose, we want the formulas capture the main features of performance caused by phase transformations. These formulas can be used to guide material development and device design. For this purpose, we introduce the model of *ideal phase transformation systems*. This model is based on the following four assumptions.

1. The entropy difference, $\Delta S = S_{\rm a}(F,\theta) - S_{\rm m}(F,\theta)$, is a constant.

   This assumption is true if both phases have the same heat capacity at any temperature and under any thermodynamic force. Since we mainly consider solid-solid phase transformation, this assumption is mild. Geometrically, it means that, in the $T-S$ diagram, the isobaric curves corresponding to each single phase (dotted and dashed lines in Fig. 1(a)) are parallel to each other. Under this assumption, the Clausius-Clapeyron

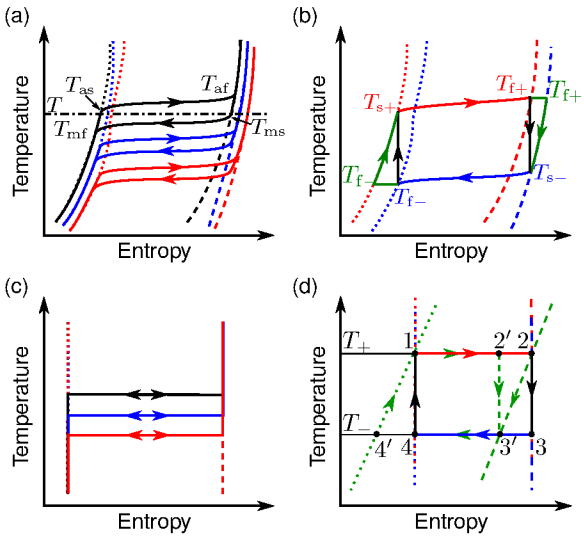

Fig. 1 (a) A schematic of the constitutive properties of a multiferroic material undergoing first order phase transformation in the temperature-entropy plane. (b) A energy conversion Rankine cycle utilizing the material. (c) The constitutive properties of an ideal phase transformation system. (d) A Rankine/Ericsson cycle (1234) for an ideal phase transformation system, and a Rankine ($12'3'4$) and an Ericsson ($123'4'$) cycle for a more realistic system. In all subfigures, dotted (resp. dashed) lines are curves corresponding to the low (resp. high) temperature single phase. Solid lines representing the effective properties of the whole material. Red, blue, and black indicate the material's behaviors under different thermodynamic forces.

relation (2) reduces to

$$\frac{dT}{dF} = -\frac{X_a - X_m}{S_a - S_m} = -\frac{X_a - X_m}{\ell / T_0}, \tag{4}$$

where ℓ and T_0 are respectively the latent heat and transformation temperature measured without applying a finite thermodynamic force. We call them the *reference latent heat* and *reference transformation temperature* respectively.

2. $\Delta X = X_a - X_m$ is independent of transformation temperature.

   This assumption relies on the fact that if the change in ferroic property X upon phase transformation is large relative to its variation with T or F in single phases. For example, the thermal-magnetic phase-transforming alloy $Ni_{45}Co_5Mn_{40}Sn_{10}$ has a jump of magnetization in the order of 10^6 A/m (1000 emu/cm^3) under zero applied magnetic field. Since the non-ferromagnetic phase has a negligible magnetization at any temperature, and the variation of the saturation magnetization of ferromagnetic phase due to a varying magnetic field or temperature is much smaller than 10^6 A/m, as long as the change of magnetic field is moderate (several Tesla) and the temperature remains well below the Curie temperature. Therefore, a slight variation of the transformation temperature due the application of magnetic field will not change the jump ΔX significantly. Numeric results of this example can be found in Ref. 21. Under this assumption, Eqn. (4) is further simplified,

$$\frac{T - T_0}{T_0} = -\frac{(X_a - X_m)F}{\ell} = -\frac{\Delta X F}{\ell}. \tag{5}$$

   In a dimensionless form, we write

$$\bar{T} = 1 - C\bar{F}. \tag{6}$$

   where $\bar{T} = T/T_0$, and $\bar{F} = F/[F]$. $[F]$ is the characteristic unit of thermodynamic force F, which will be chosen accordingly when the exact meanings of X and F are specified. The dimensionless parameter $C = \Delta X[F]/\ell$ is called the *Clausius-Clapeyron coefficient*.

   In the rest of this paper, we shall continue using the superimposed bar to denote dimensionless variables. The corresponding characteristic unit, denoted by square brackets, will be specified when a dimensionless variable with the same physical dimension first appears. For example, from now on, all dimensionless temperatures are normalized by T_0.

3. *Reversible phase transformation*: $T_{as} = T_{af} = T_{ms} = T_{mf} = T$.

   This is an assumption of zero hysteresis. It is also a consequence of the endoreversibility. Even without the assumption about endoreversibility, it is still a mild assumption for martensitic phase transformation, given the evidence that by tuning the compositions of a family of alloys, the hysteresis of such transformations can be reduced to nearly zero[35]. The justification based on the theory of "$\lambda_2 = 1$" has been discussed in the introduction. Geometrically, in $T - S$ diagram, under this assumption, isobars and isotherms coincide during phase transformation, as shown in Fig. 1(c).

4. *Zero heat capacities*: $S_a(H, T)$ and $S_m(H, T)$ are both constants.

   This is a step further than Assumption 1. Physically, it assumes that the heat capacities of two phases are not just equal but actually vanishing (negligible) simultaneously. It takes into account the observation[17,21] on typical differential scanning calorimetry measurements of such low-hysteresis solid-solid phase transformation that the peaks at transformation temperatures due to the latent heat absorbed/emitted are much

higher than the plateaus whose heights correspond to single phase heat capacities. Geometrically, the isobars of single phases in $T-S$ diagram become vertical lines (see Fig. 1(c)).

This assumption, as seen in the forthcoming sections, greatly simplifies the algebra, enables closed-form formulas of efficiency and power output, and more importantly reveals pivotal dimensionless parameters in these complex multiphysics energy conversion systems. Nevertheless, we will discuss in Sect. 2.4 the corrections of efficiency and power output when this assumption is relaxed.

Based on these assumptions, both Rankin cycles and Ericsson cycles are equivalent to Carnot cycles (Fig. 1(d)). A Carnot cycle originally has three degrees of freedom: two temperatures and one entropy difference. Here, it reduces to two because of the constrains introduced by the Clausius-Clapeyron relation (6). A convenient choice would be (T_+, T_-) or (F_+, F_-). The efficiency defined by $(3)_1$ becomes

$$\eta = 1 - \frac{T_-}{T_+} = \frac{C(\bar{F}_- - \bar{F}_+)}{1 - C\bar{F}_+}. \tag{7}$$

Since $0 \leqslant \bar{T}_- \leqslant \bar{T}_+$, the Clausius-Clapeyron relation (6) requires

$$C\bar{F}_+ \leqslant C\bar{F}_- \leqslant 1. \tag{8}$$

This is trivial when $C \leqslant 0$, but becomes a constrain on $\bar{F}_\pm$ when $C > 0$, that is, $\bar{F}_+ \leqslant \bar{F}_- \leqslant 1/C$. Notice that the sign of C is a material property.

Let the time of heating, cooling, and adiabatic processes be t_+, t_-, t_0 respectively. The power output defined by $(3)_2$ is

$$\mathscr{P} = \Delta X(F_- - F_+)/(t_+ + t_- + t_0). \tag{9}$$

Since only the values of $T_\pm$ enter into the efficiency (7), the adiabatic switching between two thermodynamic forces is irrelevant to the efficiency. It is also of little interest to the power output: it only affects the denominator in (9), and the effect is uncoupled to any other parameter. Common treatments of t_0 is either assuming that it is proportional to $t_+ + t_-$, as Curzon and Ahlborn[23] did, or simply neglecting it, as we shall do in this paper. We still cannot compute the power output until the heat transfer model is given, which will be discussed in Sect. 2.3.

2.3 Heat Transfer and Power Output

We study rate-dependent cycles by specifying the heat transfer methods for heating and cooling branches, in addition to prescribing the time evolution of the heat reservoir (environment, ambient), $\tau(t)$. In this paper, we focus on two heat transfer modes of a Rankine cycle: both heating and cooling are convective, and cooling is convective and continuous, while heating is radiative and periodic.

2.3.1 Convective heating and cooling In the first mode of heat transfer, the temperature of heat reservoir is set to be a constant τ_+ (reps. τ_-) during the heating (reps. cooling), shown as the process 12 (resp. 34) in Fig. 1(d). Thus, the heating rate as a function of time is given by

$$Q^I(t) = \begin{cases} Q^I_+ := \alpha h_+(\tau_+ - \theta_+), & t \in \mathscr{C}_+; \\ Q^I_- := \alpha h_-(\tau_- - \theta_-), & t \in \mathscr{C}_-. \end{cases} \tag{10}$$

$\mathscr{C}_\pm$ denote the time intervals of heating and cooling branches of a cycle, respectively. $h_\pm \geqslant 0$ is the heat transfer coefficient with unit of $\mathrm{W/m^2K}$, and α is the ratio of the surface for heat exchange to the volume of specimen. Here, we adopt the ideal system assumptions given in Sec. 2, so the temperature of the specimen during heating or cooling is constant too and equal to the transformation temperatures under the given thermodynamic forces, *i.e.* $\theta_+ = T_+$ and $\theta_- = T_-$. Their relations to the thermodynamic forces F_+ and F_- are also given in Eqn. (6). Clearly, we have the constrain $\tau_- \leqslant \theta_- \leqslant \theta_+ \leqslant \tau_+$. The total heat absorbed or emitted during heating and cooling are the corresponding latent heat $\ell_\pm$, respectively. According to the conservation of entropy, as a consequence of endoreversibility (also Assumption. 1), we have

$$\ell_+/\theta_+ = \ell_-/\theta_- = \ell/T_0 = \Delta S. \tag{11}$$

Fixing τ_+ and τ_-, the power output can be maximized over θ_+ and θ_-, and the maximizer is given by (see also Ref. 23),

$$\theta_\pm = \frac{1 + \sqrt{h'\tau'}}{1 + \sqrt{h'}}\sqrt{\tau_\pm \tau_+}, \tag{12}$$

where $\tau' = \tau_-/\tau_+$ and $h' = h_-/h_+$. Thus, in order to make a Carnot cycle working at maximum power output, the thermodynamic force should be set as $\bar{F}_\pm = (1 - \bar{\theta}_\pm)/C$. The maximum power output and corresponding efficiency and frequency are

$$\mathscr{P}^I_{\max} = \alpha h_+ \tau_+ \,(1 - \sqrt{\tau'})^2 \Big/ (1 + \sqrt{h'})^2, \tag{13a}$$

$$\eta^I_{\max} = 1 - \sqrt{\tau'}, \tag{13b}$$

$$f^I_{\max} = (\alpha h_- T_0/\ell)\,/\,(1 + \sqrt{h'\tau'}). \tag{13c}$$

This maximizer is universal to all endoreversible thermodynamic cycles under the working condition $\tau_\pm$. For our phase-transformation system, the only requirement is that if the Clausius-Clapeyron coefficient C is positive (resp. negative), then θ_+ (resp. θ_-) must be greater (resp. less) than the reference transformation temperature, T_0.

2.3.2 Radiative heating and convective cooling In the second heat transfer mode, the heat reservoir is kept at the temperature of τ all the time, while a radiative heating with the power of q, with the unit of W/m^2, is applied during only the heating processes of cycles. Modeling radiative heating by a constant power is a simplification of the Stefan-Boltzmann law, given the temperature of the radiation source is much higher than any possible temperature the material could experience in a cycle, such as solar-thermal or heating lamps. Then, the heating rate is given by the following piecewise constant function of time.

$$Q^{II}(t) = \begin{cases} Q_+^{II} := \alpha q + \alpha h(\tau - \theta_+), & t \in \mathscr{C}_+; \\ Q_-^{II} := \alpha h(\tau - \theta_-), & t \in \mathscr{C}_-. \end{cases} \tag{14}$$

where h is the heat transfer coefficient of the continuous convective cooling. Note that the positiveness of Q_+^{II} and negativeness of Q_-^{II} yield $\tau < \theta_- < \theta_+$.

Following the same arguments used in the preceding subsection, we maximize the power output over $\theta_\pm$ and get

$$\begin{cases} \theta_+ = \tau(1 + q' + \sqrt{1+q'})/2, \\ \theta_- = \tau(1 + \sqrt{1+q'})/2, \end{cases} \tag{15}$$

where $q' = q/h\tau$. Note that for any $q' > 0$, the aforementioned constrain $\theta_+ < q/h + \tau$ is satisfied, and therefore we are assured that $Q_+^{II} > 0$. The maximum power output and corresponding efficiency are

$$\mathscr{P}_{\max}^{II} = \alpha h \tau \left[q' + 2(1 - \sqrt{1+q'})\right] \Big/ 4, \tag{16a}$$

$$\eta_{\max}^{II} = q' \Big/ \left[1 + q' + \sqrt{1+q'}\right], \tag{16b}$$

$$f_{\max}^{II} = (\alpha h T_0/\ell) \left[q' + 2(1 - \sqrt{1+q'})\right] / 2q'. \tag{16c}$$

An interesting observation is that in Eqn. (16), the efficiency approaches 1/2 as $q' \to 0$, while in the previous result, *i.e.* Eqn. (13), it goes to 1 as $\tau' \to 0$. Both limiting cases correspond to a 0 K convective cooling.

Although both Eqns. (13) and (16) have no explicit dependence on material constants, not every material, along with an appropriate device, can perform the cycles described by the solutions (12) and (15). Finding materials (or devices) having the particular constitutive properties that match exactly the requirements of a cycle working at maximum power output is crucial for the optimization of the performance of energy conversion.

2.4 Corrections of finite heat capacity

Finally, we consider the corrections due to Assumption 4. In Fig. 1(d), the cycle 1234 is the Rankine/Ericsson cycle for an ideal phase transformation system, while the cycle $12'3'4$ and $123'4'$ are respectively the relatively more realistic (without Assumption 4) Rankine cycle and Ericsson cycle.

First, let us compare the two Rankine cycles: 1234 and $12'3'4$. From Fig. 1(d), we see that the assumption of zero heat capacities does not affect either the efficiency formula (7) or the average power output formula (9). Because, both non-ideal ($12'3'4$) and ideal (1234) cycles correspond to the same $F_\pm$, therefore the same $\theta_\pm$, which are $\theta_\pm = T_\pm$. Hence the efficiency is not affected. Power output is also unaffected because $\theta_\pm$ are the only internal parameters on which the heat transfer depends (Sect. 2.3). However, there are two minor corrections due to Assumption 4. One is that the frequency computed by the ideal system model, *i.e.* $f = 1/(t_+ + t_-)$, is actually underestimated. Because the non-ideal cycle $12'3'4$ has the same power as the ideal cycle 1234, as discussed above, but a smaller net work output, as shown by the areas enclosed by the loops in Fig. 1(d). The other correction is that it puts an bound on the difference between F_+ and F_-, or equivalently θ_+ and θ_-, because when the difference is too large, the cycle shrinks to a single vertical line , or even a loop with a "negative area".

Let the heat capacity be a constant c, and the entropy of low temperature phase at the reference transformation temperature be zero, the entropy of state 1, 2, and $2'$ are respectively

$$\begin{cases} S_1 = c \ln\left(1 - C\bar{F}_+\right), \\ S_2 = c \ln\left(1 - C\bar{F}_+\right) + \ell/T_0, \\ S_{2'} = S_{3'} = c \ln\left(1 - C\bar{F}_-\right) + \ell/T_0. \end{cases} \tag{17}$$

The ratio of real frequency to ideal frequency is the same as that of the area enclosed by 1234 to $12'3'4$, which is in terms of entropy differences

$$\frac{S_2 - S_1}{S_2' - S_1} = \frac{1}{1 + \bar{c} \ln\left[(1 - C\bar{F}_-)/(1 - C\bar{F}_+)\right]}, \tag{18}$$

where the heat capacity is normalized by $[c] = \ell/T_0$. The limiting case is that S_1 is equal to $S_{3'}$. The inequality $S_1 \leqslant S_{3'}$ leads to a constrain on F_+ and F_-,

$$(1 - C\bar{F}_-) \big/ (1 - C\bar{F}_+) \geqslant e^{-1/\bar{c}}. \tag{19}$$

It further leads to an upper bound of the efficiency:

$$\eta \leqslant 1 - \exp(-1/\bar{c}). \tag{20}$$

By comparing (18) with (19), we see that the second correction can also be interpreted as a consequence of the finiteness of frequencies in real situations.

Second, let us compare the two Ericsson cycles: 1234 and $123'4'$. Compared to the ideal cycle 1234, the realistic cycle $123'4'$ absorbs more heat from the hot reservoir (the area under the curve $4'1$), and also release more heat to the cold reservoir (the area under the curve $23'$). These two parts of

heat exchange are, with positiveness indicating heat absorption,

$$\mathscr{H}_{4'1} = c(T_+ - T_-) = \bar{c}\Delta\bar{T}\ell, \tag{21}$$
$$\mathscr{H}_{23'} = c(T_- - T_+) = -\bar{c}\Delta\bar{T}\ell. \tag{22}$$

Thus, the efficiency, different from Eqn. (7), is now

$$\eta_{\rm E} = \frac{\ell_+ - \ell_-}{\ell_+ + \bar{c}\Delta\bar{T}\ell} = \eta_{\rm C}\frac{\bar{T}_+}{\bar{T}_+ + \bar{c}}. \tag{23}$$

where the subscripts E and C denote the realistic Ericsson and the ideal — Carnot = Ericsson = Rankine — cycles, respectively. From the correction (23), we see that to make a practical Ericsson cycle closer to the ideal Carnot cycle, we need to increase the dimensionless transformation temperature upon heating $\bar{T}_+$ or to decrease the dimensionless heat capacity $\bar{c} = cT_0/\ell$.

Since $\mathscr{H}_{4'1}$ in (21) and $\mathscr{H}_{23'}$ in (22) have the same value, the total work output remains no change in the correction. We only need to consider the modification on cycling speed. In the case of convective heating and convective cooling, the time required for the four sub-processes of the cycle $123'4'$ are respectively

$$t_{4'1} = \frac{c}{\alpha h_+}\ln\frac{\tau_+ - \theta_-}{\tau_+ - \theta_+}, \quad t_{12} = \frac{\ell_+}{\alpha h_+(\tau_+ - \theta_+)},$$
$$t_{23'} = \frac{c}{\alpha h_-}\ln\frac{\theta_+ - \tau_-}{\theta_- - \tau_-}, \quad t_{3'4'} = \frac{\ell_-}{\alpha h_-(\theta_- - \tau_+)}. \tag{24}$$

In the case of radiative heating and convective cooling, $t_{23'}$ and $t_{3'4'}$ are the same as (24), while $t_{4'1}$ and t_{12} become

$$t_{4'1} = \frac{c}{\alpha h}\ln\frac{(q'+1)\tau - \theta_-}{(q'+1)\tau - \theta_+}, \; t_{12} = \frac{\ell_+}{\alpha h\left[(q'+1)\tau - \theta_+\right]}. \tag{25}$$

In either case of heat transfer mode, the power output is corrected according to

$$\mathscr{P}_{\rm E} = \mathscr{P}_{\rm C}\frac{t_{12} + t_{3'4'}}{t_{4'1} + t_{12} + t_{23'} + t_{3'4'}}. \tag{26}$$

Because the net heat absorption is the same in both practical and ideal cycles, the correction of frequency is exactly the same as power output.

3 Thermomagnetic Phase Transformation

3.1 Material consideration: thermomagnetic energy conversion

The alloy $Ni_{44}Co_6Mn_{40}Sn_{10}$, as well as its nearby compositions, undergoes a first order martensitic phase transformation from an antiferromagnetic martensite to a ferromagnetic austenite phase upon heating[17,47]. During the transformation, its magnetization increases about $\Delta M = 10^6$ A/m. The latent heat and transformation temperature at zero-field measured by differential scanning calorimetry (DSC) are respectively about $\ell = 10^8$ J/m^3 and $T_0 = 400$ K. With these three material constants, among other parameters listed in Table 1, we can make some analytic predictions based on the ideal system assumptions.

In this case, as shown by Song *et al.*[21] to be a good approximation of the full 3D continuum theory, $X = M$ and $F = \mu_0 H$, where M is magnetization, H is the *external* magnetic field, and μ_0 is the vacuum permeability. Given that $\Delta M > 0$, the characteristic unit of F can be chosen as $[F] = \mu_0\Delta M$, so that $\bar{F} = H/\Delta M := \bar{H}$, *i.e.* $[H] = \Delta M$. Note that such choice of $[F]$ is not unique. Other common choices of $[F]$ include $\mu_0 M_{\rm s}$ and H_0 with $M_{\rm s}$ being the saturation magnetization of austenite, and H_0 is a reference magnetic field strength, such as the background field generated by a permanent magnet. We choose $\mu_0\Delta M$ because the resulting Clausius-Clapeyron coefficient is a pure material constant. In fact, all the following analysis is valid for any choice of $[F]$. If the material is modeled by an ideal system, the Clausius-Clapeyron relation reads, according to Eqn. (6),

$$\bar{T} = 1 - C\bar{H}, \tag{27}$$

where the dimensionless Clausius-Clapeyron coefficient, in this case, becomes $C = \mu_0(\Delta M)^2/\ell$. Note that this C is positive. The efficiency of an ideal Rankine cycle, as given by Eqn. (7), is then

$$\eta = \frac{C(\bar{H}_- - \bar{H}_+)}{1 - C\bar{H}_+}. \tag{28}$$

Without loss of generality, we can write $\bar{H}_\pm = \bar{H}_0 \pm \Delta\bar{H}$ for some $\bar{H}_0$ and $\Delta\bar{H}$.

3.2 Device consideration: thermoelectric energy conversion

A nearby alloy $Ni_{45}Co_5Mn_{40}Sn_{10}$ was demonstrated as a potential candidate for direct energy conversion from heat to electricity[11]. In the demonstration (Fig. 2), as well as its generalized versions discussed below, an axisymmetric specimen of the alloy is placed in a uniform background field – generated by a permanent magnet – and surround by a pick-up coil. The coil is connected to a load that is modeled by a resistor here. We drive the phase transformation by the two heat transfer modes discussed in Sect. 2.3. During the phase transformation, the change in magnetization generates a current in the pick-up coil due to Faraday's law of induction, and this coil further induces a *back-field* on its core region.

We use the thermodynamics and heat transfer models developed above to analyze the performance of this kind of energy conversion devices. The thermomagnetic cycles of the

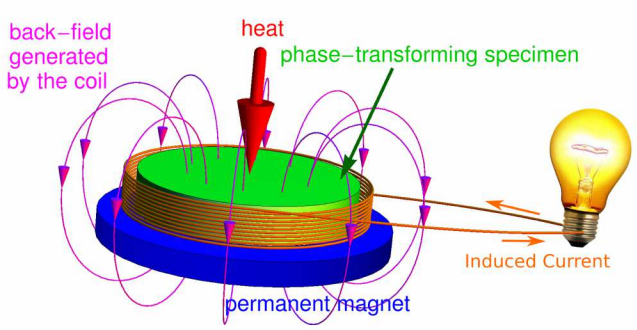

Fig. 2 A schematic view of the energy conversion device. Reproduced from Ref. 21 with permission from The Royal Society of Chemistry.

working material in such devices are the same as described above with $\bar{H}_0$ being the background field and $\Delta\bar{H}$ being the back-field. As proven in Ref. 21, in this setting, the magnetic work done by the back-field on the alloy is equal to the electricity delivered to the load. By studying the thermomagnetic cycles, we can evaluate the performance of the thermoelectric conversion. A major difference between the cycles considered in this section and those mentioned in previous sections is that the thermodynamics forces are no longer independent parameters of a cycle. Instead, it now depends on the heat transfer. Roughly speaking, a faster heat transfer generates a stronger back-field $\Delta\bar{H}$, *vice versa*. The exact dependence of $\Delta\bar{H}$ on the heat transfer rate can be derived starting with Ampère's and Faraday's laws in electromagnetism.

According to Ampère's law, the vector back-field generated by the coil is a linear function of the current, *i.e.*,

$$\mathbf{H}_{\mathrm{b}}(\mathbf{x}) = \mathbf{l}(\mathbf{x})I, \tag{29}$$

where the vector field $\mathbf{l}$ is the coefficient of the proportionality, which only depends on the geometry of the coil. Note that $\mathbf{l}$ is inhomogeneous but varying slowly at the center of the core region. For a full loop of wire in the coil, whose enclosing area is $\mathscr{O}$, Faraday's law reads

$$\int_{\partial\mathscr{O}} \mathbf{E}\cdot d\boldsymbol{\ell} = -\int_{\mathscr{O}} \dot{\mathbf{B}}\cdot\mathbf{n}\,da, \tag{30}$$

where the vectors $\mathbf{E}$ and $\mathbf{B}$ are electric field and magnetic induction respectively. When the coil contains N turns, denoted $\mathscr{O}_i$, $i = 1,2,\cdots,N$, the induced electromotive force is

$$\begin{aligned} V &= \int_{\mathscr{W}} \mathbf{E}\cdot d\boldsymbol{\ell} = \sum_{i=1}^{N}\int_{\partial\mathscr{O}_i} \mathbf{E}\cdot d\boldsymbol{\ell} = -\sum_{i=1}^{N}\int_{\mathscr{O}_i} \dot{\mathbf{B}}\cdot\mathbf{n}\,da, \\ &= -\mu_0\sum_{i=1}^{N}\int_{\mathscr{O}_i} (\dot{\mathbf{H}}_{\mathrm{b}} + \dot{\mathbf{H}}_{\mathrm{m}} + \dot{\mathbf{M}})\cdot\mathbf{n}\,da. \end{aligned} \tag{31}$$

where $\mathscr{W}$ is the center-line path of the coil and the vector $\mathbf{H}_{\mathrm{m}}$ is the demagnetization field generated by the magnetization. We have used the dipolar relation $\mathbf{B} = \mu_0(\mathbf{H}_0 + \mathbf{H}_{\mathrm{b}} + \mathbf{H}_{\mathrm{m}} + \mathbf{M})$ and the fact that the background field is constant. To evaluate the last term, note that because the M define in Sect. 3.1 is the volume averaged magnetization, and the demagnetization field $\mathbf{H}_{\mathrm{m}}$ is proportional to M, we have a good approximation

$$\begin{aligned} &\mu_0\sum_{i=1}^{N}\int_{\mathscr{O}_i} (\dot{\mathbf{H}}_{\mathrm{m}} + \dot{\mathbf{M}})\cdot\mathbf{n}\,da \\ =&\mu_0 NA\frac{1}{|\Omega|}\frac{d}{dt}\int_0^L\int_{\mathscr{O}_i} \mathbf{H}_{\mathrm{m}} + \mathbf{M}\,da\,dx\cdot\mathbf{n} \\ \approx&\mu_0(1-\delta)NA\dot{M}, \end{aligned} \tag{32}$$

where A is the cross-section area of the specimen (distinct from the surface area for heat transfer), and $\delta \in (0,1)$ is the demagnetization factor along the direction of magnetization. δ approaches to its limiting value of 1 (resp. 0), as the shape of the specimen approaches to a thin sheet (resp. thin rod). Suppose the specimen is in the shape of a cylinder with the basal area of A and the height of h, placed in coil co-axially (see Fig. 2 and the insets of Fig. 4). Denote the aspect ratio of the specimen $\gamma := \mathsf{h}/2\sqrt{A/\pi}$, the demagnetization factor δ is well approximated by[48]

$$\delta(\gamma) = \begin{cases} \dfrac{1}{\gamma^2-1}\left[\dfrac{\gamma}{\sqrt{\gamma^2-1}}\ln\left(\gamma+\sqrt{\gamma^2-1}\right)-1\right], & \gamma > 1, \\ 1-\dfrac{\gamma}{1-\gamma^2}\left[\dfrac{\arccos\gamma}{\sqrt{1-\gamma^2}}-\gamma\right], & \gamma < 1. \end{cases} \tag{33}$$

Eqns. (29), (31), and (32) imply an ordinary differential equation for the current,

$$IR = V = -\mu_0\left(\sum_{i=1}^{N}\int_{\mathscr{O}_i}\mathbf{l}\cdot\mathbf{n}\,da\right)\dot{I} - \mu_0(1-\delta)NA\dot{M}. \tag{34}$$

Here R is the total resistance of the coil and the external load. If the resistance of the coil is non-negligible, the real efficiency and power output are fractions of the values calculated below.

The term in the first pair of parenthesis on the right hand side of (34) is the inductance of the coil in air. Closed form formulas of the inductance can be computed for many types of coils, as given, for example, by Terman[49]. For a finite size coil with the length of d and the inner/outer radius of $r_{\mathrm{i}}/r_{\mathrm{o}}$, the approximation of inductance can be obtained from Biot-Savart's law,

$$\begin{aligned} \mathscr{L} &\equiv \sum_{i=1}^{N}\int_{\mathscr{O}_i}\mathbf{l}\cdot\mathbf{n}\,da \\ &\approx \frac{\pi\bar{r}wN^2}{2\hat{w}}\ln\left(\frac{2(w+\hat{w})+\sqrt{1+4(w+\hat{w})^2}}{2w+\sqrt{1+4w^2}}\right), \end{aligned} \tag{35}$$

where $\bar{r} = (r_o + r_i)/2$ is the average radius, $w = 2r_i/d$ is the (inner) aspect ratio, and $\hat{w} = 2(r_o - r_i)/d$. For a single layer solenoid, *i.e.* $\bar{r} = r_i = r_o$, Eqn. (35) leads to the asymptotic formulas[50]:

$$\mathscr{L} \approx \begin{cases} \pi r w N^2/2, & w \ll 1; \\ r N^2, & w \gg 1. \end{cases} \tag{36}$$

The key observation on the asymptotic formulas is that for a long coil ($w \ll 1$), $\mathscr{L}$ depends linearly on w, while for a short coil ($w \gg 1$), it is independent of w and therefore suffers no singularity as $w \to \infty$.

3.3 Efficiency and the figure of merit

To solve the Eqn. (34) for the current, we need a relationship between $\dot{M}$ and I. This relationship is affected by micromagnetic phenomena and the kinetics of phase transformation. Given that little is known about the latter, even for an ideal system, we make the following simple hypothesis of stationary evolution, *i.e.*, $\dot{M}$ is a constant. With these assumptions either the heating or the cooling process yields an explicit solution to (34) given by

$$\begin{aligned} I(t) = &- e^{-Rt/\mu_0\mathscr{L}}[I(0) - \mu_0(1-\delta)NA\dot{M}/R] \\ &- \mu_0(1-\delta)NA\dot{M}/R, \end{aligned} \tag{37}$$

where $I(0)$ is the initial condition at the beginning of heating or cooling. Given the inductance of the coil as in Eqn. (36), when r is in the scale of cm, N is several hundred, and R is 1 Ohm, $R/\mu_0\mathscr{L}$ is then in the order of $10^3 - 10^4$ Hz. When the time scale of the phase transformation is much slower than this time constant, *i.e.* the frequency satisfies $f \ll R/\mu_0\mathscr{L}$, the solution (37) is well approximated by its asymptote, or say the upper bound in the sense of power output, $I = -\mu_0(1-\delta)NA\dot{M}/R$. Due to the equivalence of magnetic work and electricity,[21] in a full cycle, the average electric power output converted from heat is $\mathscr{P} = \oint_{\mathscr{C}} I^2 R\, dt = -\oint_{\mathscr{C}} \langle \mu_0 \mathbf{H}_b \cdot \dot{\mathbf{M}} \rangle_\Omega\, dt$. Here, the angled brackets denote volume averages, and the dashed integral symbols denote time averages. Now we have $\langle \mu_0 \mathbf{H}_b \cdot \dot{\mathbf{M}} \rangle_\Omega = -\mu_0^2(1-\delta)^2 N^2 A\dot{M}^2/R\mathrm{h}$. Let the stationary change of magnetization in heating and cooling processes be $\dot{M}_+ > 0$ and $\dot{M}_- < 0$ respectively, the thermodynamic forces to be used in the Clausius-Clapeyron relation are therefore

$$\mu_0 \bar{H}_\pm = \mu_0 \bar{H}_0 - \mu_0 \Pi \dot{\bar{M}}_\pm, \tag{38}$$

where $\bar{M} = M/\Delta M$, and $\Pi = \mu_0(1-\delta)^2 N^2 A/R\mathrm{h}\bar{H}_0$. Hence, $\dot{\bar{M}}_\pm$ have the dimension of time^{-1}, and Π has that of time. The efficiency as given by Eqn. (28) is

$$\eta = \frac{C\Pi(\dot{\bar{M}}_+ - \dot{\bar{M}}_-)}{1 - C\bar{H}_0 + C\Pi\dot{\bar{M}}_+}. \tag{39}$$

The power output is

$$\mathscr{P} = -\ell C \Pi \dot{\bar{M}}_+ \dot{\bar{M}}_-, \tag{40}$$

and the corresponding frequency is

$$f = \dot{\bar{M}}_+ \dot{\bar{M}}_- \Big/ \left(\dot{\bar{M}}_- - \dot{\bar{M}}_+\right). \tag{41}$$

If the heat transfer method is specified, we can compute $\dot{\bar{M}}_\pm = Q_\pm/\ell_\pm$. Here, we discuss the two modes of heat transfer introduced in Sect. 2.3. In the first mode, $Q_\pm$ are given by Eqn. (10). Combining Eqns. (10),(11) and (27), under the help of (38), we obtain a pair of equations for $\dot{\bar{M}}_\pm$. Solving them for $\dot{\bar{M}}_\pm$ leads to

$$\dot{\bar{M}}_\pm = g(zz'_\pm, \hat{\tau}_\pm)(1 - C\bar{H}_0)/2C\Pi, \tag{42}$$

where $\hat{\tau}_\pm = \bar{\tau}_+/(1 - C\bar{H}_0)$, $z'_- = h' = h_-/h_+$, $z'_+ = 1$, and the dimensionless function $g(z,\tau)$ is defined as

$$g(x,y) := -x - 1 + \sqrt{(x+1)^2 + 4x(y-1)}. \tag{43}$$

Note that g is positive (resp. negative) and monotonically increasing (resp. decreasing) in x when $y > 1$ (resp. $y < 1$), and it is identically zero when $y = 1$. We name the dimensionless parameter

$$z = \frac{C\Pi\alpha h_+ T_0}{(1 - C\bar{H}_0)\ell} \tag{44}$$

the *figure of merit* of such an energy conversion device using the given material and the given heat transfer mode. Tow time scales are involved in the figure of merit: the electromagnetic time scale Π and the heat transfer time scale $\ell/\alpha h_+ T_0$. Under these definitions, the efficiency (39) can be rewritten as a function of $\hat{\tau}_\pm$, $z'_\pm$ and z, *i.e.*

$$\eta = \frac{g(zz'_+, \hat{\tau}_+) - g(zz'_-, \hat{\tau}_-)}{2 + g(zz'_+, \hat{\tau}_+)}. \tag{45}$$

Similarly, the power output (40) and the frequency (41) reduce to

$$\hat{\mathscr{P}} := \mathscr{P}\ell/(1 - C\bar{H}_0)\bar{h}_+ = -g(zz'_+, \hat{\tau}_+)g(zz'_-, \hat{\tau}_-)/4z, \tag{46}$$

$$\hat{f} := \frac{2C\Pi f}{(1 - C\bar{H}_0)} = \frac{-g(zz'_+, \hat{\tau}_+)g(zz'_-, \hat{\tau}_-)}{g(zz'_+, \hat{\tau}_+) - g(zz'_-, \hat{\tau}_-)}. \tag{47}$$

Recall that the thermodynamic force must be non-negative, Eqn. (38) requires $\Pi\dot{\bar{M}}_+ \leqslant \bar{H}_0$, which introduces a constrain on $\hat{\tau}_+$, according to Eqn. (42),

$$g(zz'_+, \hat{\tau}_+) < 2C\bar{H}_0/(1 - C\bar{H}_0). \tag{48}$$

Another constrain caused by the correction of non-zero heat capacities, *i.e.* Eqn. (18), is

$$\frac{1+g(zz'_+,\hat{\tau}_+)/2}{1+g(zz'_-,\hat{\tau}_-)/2} \geqslant e^{-1/\bar{c}}. \tag{49}$$

Since $g(zz'_+,\hat{\tau}_+) > 0$ and $g(zz'_-,\hat{\tau}_-) < 0$, (49) is mild when $\bar{c} < 1$ is small.

If, instead, the second heat transfer mode, Eqn. (14), is used, the solutions for $\dot{M}_\pm$ are still in the form of Eqn. (42) but with different parameters: $z'_\pm = 1$, $\hat{\tau}_- = \bar{\tau}/(1-C\bar{H}_0)$, $\hat{\tau}_+ = (\bar{\tau}+q/hT_0)/(1-C\bar{H}_0)$. The figure of merit is the same as Eqn. (44), except h_+ is now replaced by h. The efficiency and power output are given by the same equations, (45) and (46) respectively.

Since $\lim_{x\to\infty} g(x,y) = 2(y-1)$, the Carnot efficiency is recovered as $z\to\infty$, *i.e.* $\lim_{z\to\infty}\eta = 1-(\hat{\tau}_-/\hat{\tau}_+) = 1-(\tau_-/\tau_+)$. But the effective power output vanishes, *i.e.* $\lim_{z\to\infty}\hat{\mathscr{P}} = 0$. By plotting the efficiency and power output with varying z in Fig. 3, we confirm the above two claims and observe a maximum power output occurring at some critical value of z. For the constants used in Fig. 3, which are $z'_\pm = h' = 1$, this critical value of z is 1. Moreover, we find that the C-A efficiency[23] is recovered when $z = 1$, again with the constants used in the plotting. We also compare to the efficiency of thermoelectric materials based on Seebeck effect. The efficiency of thermoelectric materials is given by the formula[51]:

$$\eta_{\rm TE} = \frac{T_+ - T_-}{T_+}\frac{\sqrt{1+Z\bar{T}}-1}{\sqrt{1+Z\bar{T}}+T_+/T_-} \tag{50}$$

where $\bar{T} = (T_+ + T_-)/2$, $Z\bar{T}$ (or simply ZT) is the so-called *figure of merit* for thermoelectric materials. The value of ZT depends on the Seebeck coefficient, the electric and thermal conductivity of the material, in addition to the working temperatures. For most of the existing thermoelectric materials, ZT is less than 2 in a wide range of temperature[52]. In Fig. 3, we choose $ZT = 2$ for the comparison.

z depends on the shape of specimen, in particular the aspect ratio γ, because factors such as Π, α and A/h are geometry-dependent. We consider two types of configurations where the shape-dependence of z can be explicitly derived (Fig. 4).

a) A disk with heat transfer through the top surface (Fig. 4(a))

The surface-volume ratio of heat transfer for this configuration is then simply $\alpha = 1$/h, Thus, the shape-dependence of z is

$$z \propto [1-\delta(\gamma)]^2/\gamma^2. \tag{51}$$

By plotting it in Fig. 4(a), we conclude that the best aspect ratio for this configuration is thin film, *i.e.* $\gamma \to 0$, where the value of the geometry factor is $\lim_{\gamma\to 0}[1-\delta(\gamma)]^2/\gamma^2 = \pi^2/4$.

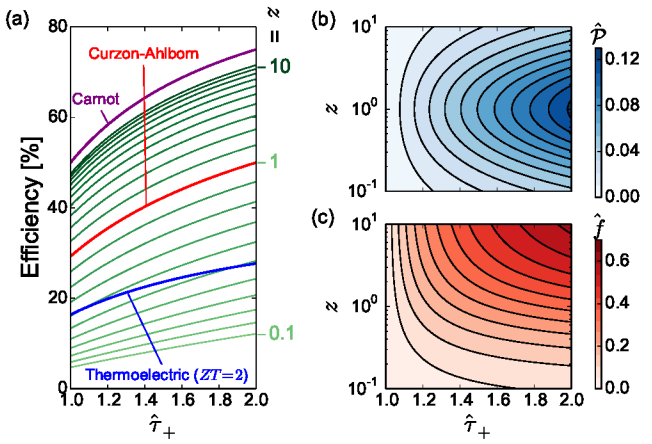

Fig. 3 (a) Efficiency, (b) effective power output, and (c) effective frequency of the proposed device with the figure of merit varying from 0.1 to 10. In (a), green thin solid lines are the efficiency for the thermal-magnetic generators with different z values. The z value increases from 0.1 to 10, as the efficiency curve moves from bottom to top. The purple and red thick solid curves represent the Carnot and Curzon-Ahlborn[23] (C-A) efficiencies, respectively. The blue thick solid curve corresponds to thermoelectric generators with the ZT value of 2. (b) and (c) are contour plots. In all of these plots, we choose $z'_\pm = h' = 1$ and $\hat{\tau}_- = 0.5$.

b) A cylinder with heat transfer through the side surface (Fig. 4(b))

In this configuration, the surface-volume ratio of heat transfer is $\alpha = 2/\sqrt{A/\pi}$. The shape-dependence of z becomes

$$z \propto 4[1-\delta(\gamma)]^2/\gamma. \tag{52}$$

The coefficient 4 is chosen so that the shape-independent part of z is the same in both configurations. Because it is γ in the denominator for the second configuration while γ^2 for the first one, large γ's prefer the second configuration while small γ's prefer the first one. However, as shown in Fig. 4(b), a nano-wire, *i.e.* $\gamma\to\infty$ ($1/\gamma\to 0$), is not the best shape for the second configuration. Instead, there exists an optimized aspect ratio near $\gamma = 0.7$ ($1/\gamma = 1.4$).

After all, the shape-dependence of z exhibits no singularity for any γ. However, the dimensional power output $\mathscr{P}$, as given in (46), has one more dependence on the surface-volume ratio α, and therefore might exhibit singularities at some extreme geometries. So, it is power output rather than efficiency that is more sensitive to the tuning of the aspect ratio.

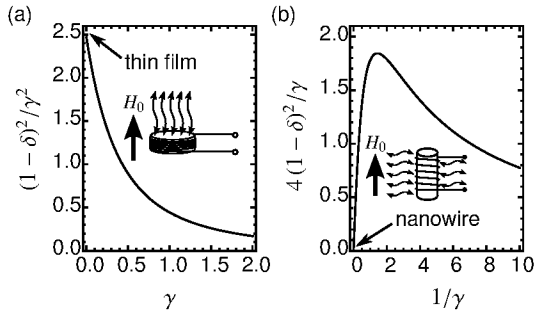

Fig. 4 Shape-dependence of the figure of merit for devices with heat exchanging through the (a) top or (b) side surface. In the insets, the cylinder represents the specimen which is surrounded by a coil, the curly double arrows indicate the surface of heat-exchange, and the bold arrow shows the direction of the background magnetic field.

3.4 Energy conversion at maximum power

On the one hand, in Sect. 2.3, we found that when working conditions, *i.e.* h's, τ's and q, are fixed, there exists a pair of θ_+ and θ_- providing the maximum power. On the other hand, in the Sect. 3.3, we saw that once the material constants and design parameters, such as z, are fixed, the same set of working conditions also predicts θ_+ and θ_-, as well as its efficiency and power output. These two sets of $\theta_\pm$ are not necessarily the same for generic material constants and design parameters. Thus, there is an issue about matching. We name it the *design-task matching* problem. We call the set of material constants and design parameters the *most suitable device* to work under certain working (heat transfer) conditions, if such device can perform the predicted maximum-power cycle. In the same fashion, we can define the *best working conditions* for a given design, *i.e.* material constants + design parameters. This subsection focuses on such design-task matching.

First, consider the case of convective heating and cooling. Comparing the results in Sect. 2.3 and Sect. 3.3, more specifically using (12), (27), (38) and (42), we have

$$1+g(zz'_\pm,\hat{\tau}_\pm)/2=\frac{1+\sqrt{h'\tau'}}{1+\sqrt{h'}}\sqrt{\hat{\tau}_\pm\hat{\tau}_+}. \tag{53}$$

Eqn. (53) are the matching criteria for the first heat transfer mode. That is because when the figure of merit z and the working conditions $z'_\pm$, h' and $\hat{\tau}_\pm$ satisfying (53), there exists a pair of $\theta_\pm$ solves the thermodynamic system (27), (38) and (42), and, at the same time, provides the maximum power among all possible energy conversion systems under the same working condition, (12).

Eqn. (53) does not always have a non-trivial solution of $\hat{\tau}_\pm$, for given z, $z'_\pm$ and h'. But we can find the region of z where such non-trivial solution exists. To begin with, let us consider two special cases: i) $\hat{\theta}_+$ and $\hat{\theta}_-$ coincide, and ii) $\hat{\theta}_-$ in the solution approaches zero. Here $\hat{\theta}_\pm=\bar{\theta}_\pm/(1-C\bar{H}_0)$. In case i), $\hat{\tau}_+$ and $\hat{\tau}_-$ must coincide too, as a proposition from Eqn. (12). So let $\hat{\tau}_+=1+\epsilon$ and $\hat{\tau}_-=1-\kappa\epsilon$, for some $\kappa,\epsilon>0$ where ϵ is small. Expanding (53) to the first order in ϵ leads to a pair of equations whose solution is $\kappa=1$, $z=1/\sqrt{h'}$. This gives one bound on z for the existence of non-trivial solutions, which is $1/\sqrt{h'}$. For case ii), let $\hat{\tau}_-=0$, then solving $\hat{\theta}_-=0$ for z leads to the second bound on z that is $1/h'$. The relative size of two bounds depends on whether h' is greater or less than 1. In either case, we can write

$$\min\{1/\sqrt{h'},1/h'\}\leqslant z\leqslant\max\{1/\sqrt{h'},1/h'\}. \tag{54}$$

Consequently, when $h'=1$, *i.e.* the same fluid manifold is used for heating and cooling, the figure of merit z must be strictly 1. It puts a quite rigid constrain on the design-task matching. Solutions to the matching equation (53) with $h'=0.2$ and 2 are plotted in Fig. 5. The intersections between a vertical line and the $\hat{\tau}_\pm$ curves suggest a design-task matching: the best working temperatures are their vertical coordinates, and the most suitable design is characterized by their common horizontal coordinate.

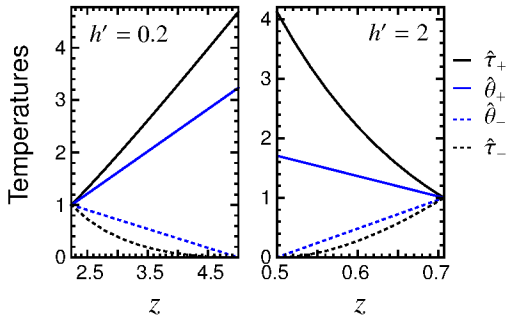

Fig. 5 Solutions to the design-task matching with convective heating and cooling, and $h'=0.2$ (left) or 2 (right). In each subfigure, the four curves from top to bottom are respectively $\hat{\tau}_+$, $\hat{\theta}_+$, $\hat{\theta}_-$ and $\hat{\tau}_-$.

Second, consider the mode of convective cooling and radiative heating. The modified Eqn. (53), according to (15), (27), (38) and (42), is now

$$\begin{cases}1+g(z,\hat{\tau})/2=\hat{\tau}(1+\sqrt{1+q'})/2,\\ 1+g(z,\hat{\tau}(1+q')/2=\hat{\tau}(1+q'+\sqrt{1+q'})/2.\end{cases} \tag{55}$$

Eqn. (55) are the matching criteria for the second heat transfer mode.

By observation, we find that

$$q'=\left(\frac{1-z-\hat{\tau}-\sqrt{(z-1)^2+4z\hat{\tau}}}{\hat{\tau}}\right)^2-1 \tag{56}$$

solves both equations in (55) simultaneously, regardless of z. Thus, for each $\hat{\tau} \in (0,1)$, there is a family of solutions to the design-task matching. The only constrain is $\hat{\theta}_+ > 1$, which reduces to

$$z < \left(\hat{\tau} + 3\sqrt{\hat{\tau}} + 2\right)\Big/ 2. \tag{57}$$

Or, if $z > 0$ is given, the constrain on $\hat{\tau}$ is

$$\begin{cases} 0 < \hat{\tau} < 1, & 0 < z \leqslant 1, \\ \dfrac{5+4z-3\sqrt{1+8z}}{2} < \hat{\tau} < 1, & 1 < z < 3, \\ \hat{\tau} \notin (0,1), & z \geqslant 3. \end{cases} \tag{58}$$

Both (57) and (58) suggest that $z < 3$. In Fig. 6, we plot the region in $z - \hat{\tau}$ plane where the design-task matching (55) has non-trivial solutions.

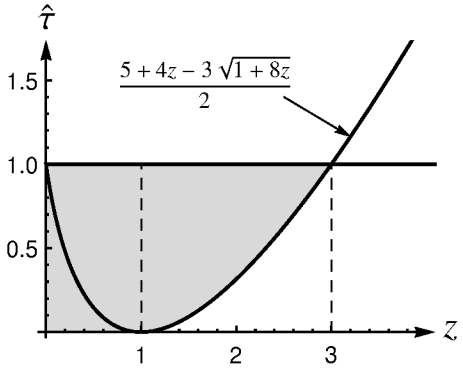

Fig. 6 The region in $z - \hat{\tau}$ plane where a solution to the design-task matching with radiative heating and convective cooling can be found.

3.5 Real materials

In Table 1, we list the material properties close to those of the alloy $Ni_{44}Co_6Mn_{40}Sn_{10}$, as well as other realistic design parameters and heat transfer conditions. The configuration of the device corresponds to the inset of Fig. 4(a). The heat transfer coefficients are the typical values of enforced or free convection by common fluids.

The Clausius-Clapeyron coefficient computed from these parameters is $C = 0.01$, which is positive. The parameter $\Pi = 7.6 \times 10^{-6}$ s, which is quite small. Unsurprisingly, the figure of merit, $z = 3.1 \times 10^{-5}$, is small too. As a consequence, the efficiency will also be low. Even worse, it is difficult to solve the design-task matching, at least with convective heating and cooling, for this extremely small z, as it is likely to be out of the range between $1/\sqrt{h'}$ and $1/h'$ mentioned in Sect. 3.4. Thus, improving the figure of merit to around the order of 1 is undoubtedly one of the most urgent tasks for future works.

parameter	description	value	unit
ΔM	change of magnetization	10^6	A/m
ℓ	latent heat at zero-field	10^8	J/m^3
T_0	transformation temperature	400	K
A	basal area of the cylinder	4π	cm^2
h	height of the cylinder	10	μm
$\mu_0 H_0$	background magnetic field	1	T
N	number of turns in the coil	500	
R	resistance of the load	1	Ohm
h_+	heat transfer coefficient	1000	W/m^{2}K
h_-	heat transfer coefficient	200	W/m^{2}K

Table 1 Parameters used in the example. The first group contains material constants which are approximately those of $Ni_{44}Co_6Mn_{40}Sn_{10}$ [21]. The second group contains design parameters. The third group contains heat transfer coefficients for heating and cooling.

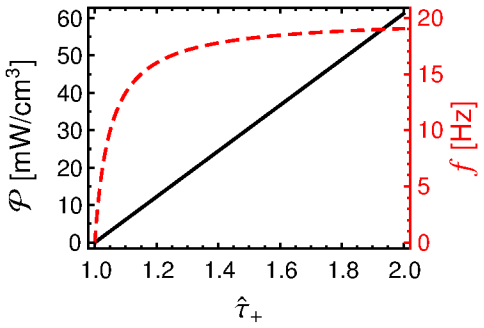

Fig. 7 The power output density (black solid line and the left axis) and the frequency (red dashed line and the right axis) of a design based on realistic parameters, as listed in Table. 1.

However, even for such a low-z material, it is still possible to obtain a good performance in terms of the power output. The power output and frequency with convective heating and cooling for parameters listed in Table 1 are plotted in Fig. 7, where we see that the power output density is in the order of 10 mW/cm^3. A similar result can be obtained by studying the other method of heat transfer. Note that the major limitation on the frequency is the cost of switching between the heating and cooling processes. For that, a frequency less than 10 Hz would be considered feasible. Our goal here is to retain, or increase, the power output while reducing the frequency to less than 10 Hz.

When x is in the vicinity of zero, the g-function can be linearized as $g(x,y) = 2x(y-1) + \mathcal{O}(x^2)$. Substituting its linear

part into Eqns. (46) and (47) gives

$$\begin{cases} \mathscr{P} = (\alpha h_+ T_0 z)(1 - C\bar{H}_0) h'(\hat{\tau}_+ - 1)(1 - \hat{\tau}_-), \\ f = \dfrac{\alpha h_+ T_0}{\ell} \dfrac{h'(\hat{\tau}_+ - 1)(1 - \hat{\tau}_-)}{(\hat{\tau}_+ - 1) + h'(1 - \hat{\tau}_-)}. \end{cases} \tag{59}$$

Excluding terms that are always in the order of 1, our task reduces to fixing, or improving, $\alpha h_+ T_0 z$ while lowering $\alpha h_+ T_0/\ell$. For that, our strategy boils down to two steps: i) decrease $\alpha h_+ T_0/\ell$ by any possible method; ii) if the power output is unaffected or increased during the first step, we are done. Otherwise, tune those parameters other than α, h_+, T_0 or ℓ to raise the power back. Note that among those parameters, we are most likely to manipulate N and R. Some examples of such a strategy are listed in Table 2.

From Table 2, we see that our simple strategy works, and the following two interesting observations are found. First, by comparing Case 1 with Case 2, we see that increasing N and decreasing R have about the same effect on the improvement of performance. The latter is much easier, once we realize that decreasing R is equivalent to distributing the load to multiple units, until R is close to the resistance of the coil in one unit. It also suggests that using a large number of units simultaneously might be a way to increase z to the order of 1. Second, although increasing the latent heat ℓ can directly decreases the frequency, but it is evident from Case 4 and 5 that lowering ℓ is actually much more favorable from the point of view of the power output. That is because the increasing ℓ raises the Clausius-Clapeyron coefficient and, subsequently, the figure of merit z. This might also give us some clue of bringing z to the order of 1.

Fig. 7 and Table 2 are calculated using the model and the parameters listed in Table 1. The only existing experimental data to compare with is the demonstration done by Srivastava *et al.*[11]. The material properties and design parameters for the demonstration are provided in Ref. 11. The authors only reported electric signal during the heating half cycle. Using their data corresponding to the first order phase transformation (the original data also has a part related to a second order phase transformation) and assuming a symmetric cooling half cycle in terms of electric signal, the efficiency is about 0.97×10^{-11} and the power density is about 4.83×10^{-8} mW/cm^3. The figure of merit can also be calculate based on values provided in Ref. 11: $z \approx 6.9 \times 10^{-10}$. Using (45) and (46), the theory predicts an efficiency of 2.53×10^{-10} and a power density of 2.49×10^{-7} mW/cm^3 for an ideal phase transformation system. Unsurprisingly, the ideal theory overestimates the performance. Since the cycle performed in the demonstration is Ericsson-like cycle with convective heating and cooling, the efficiency and the power density can be corrected by (23) and (26), where $\bar{T}_+ \approx 1.33$ and $\bar{c} \approx 9.6$. (Here we see that this alloy's heat capacity is unfavorably large compared to the ideal model.) After correction, the efficiency becomes approximately 3.04×10^{-11}. The power density is not expected to change significantly by this correction because in the slow transformation cycle (about 40 sec per cycle), $\bar{\theta}_-$ and $\bar{\theta}_+$ are very close to each other: $t_{4'1}$ and $t_{23'}$ are small compared to t_{12} and $t_{3'4'}$. The remaining error could come from practical issues such as that the coil is not tightly winded, that the heat transfer is not ideal, and that the average magnetization jump is lower than the theoretical value which is the maximum value, due to the formation of microstructure and domain structure. To conduct a meaningful validation of the model, more sophisticated and better performing prototypes, *i.e.* having the efficiency and power output not as extremely small as the previous demonstration, are necessary.

Unfortunately, there are no such experimental data available at this time. To do such experiments, we need a material with properties listed as the first three rows of Table 1, such as an alloy in the family NiCoMnSn. Then one needs to build a device with parameters listed as the next five rows in Table 1, or modified according to Table 2. According to standard data for heat transfer coefficients[53], the values listed in Table 1 can be achieved by forced and free convective heat transfer with air. One thing to keep in mind is that the final apparatus must have the ability to track heat and work input and output accurately for the whole device, in order to compare with the thermodynamic analysis.

The most difficult part of these measurements is likely to be the measurement of the heat input and output of the whole device, which may require a whole-device calorimeter. We note that if energy is consumed by a device to supply hot air, this contribution must be included in the work consumed, and the effect is to lower the overall efficiency. A simple but less accurate way to estimate the heat input is to use the measured latent heat of the material, scaled to the actual size. This may not be sufficiently accurate because (i) the DSC rate will usually differ from the actual rate of heat transfer, (ii) the DSC measurement is typically done with no applied field, (iii) the "tails" in a heat flow vs. temperature graph from DSC are difficult to estimate, (iv) the dissipation due to twin boundary and magnetic domain wall boundary motion may be different in a DSC machine than in the actual device. The power output can be directly monitored by a voltage or current meter, as long as the internal and external resistance are measured accurately.

4 Conclusions

This paper studies the efficiency and power output of energy conversion using first order phase transformation in a multiferroic material. The efficiency of converting heat into the associated ferroic property of the material, such

	step i	step ii	$\mathscr{P}$ [mW/cm^3]	f [Hz]	z
	original parameters in Table 1		31	18	3.1E-6
1	h → 100 μm	$N \to 2000$	48	1.8	4.9E-4
2	h → 100 μm	$R \to 0.1$ Ohm	30	1.8	3.1E-4
3	$T_0 \to 300$ K, h → 50 μm	$R \to 0.1$ Ohm	34	2.7	2.3E-4
4	$\ell \to 10^9$ J/m^3	$R \to 0.1$ Ohm	3.1	1.8	3.1E-6
5	$\ell \to 10^7$ J/m^3, h → 500 μm	$R \to 0.1$ Ohm	546	3.6	0.032
6	$\ell \to 10^7$ J/m^3, h → 100 μm	$R \to 0.1$ Ohm	2864	18	0.034

Table 2 Examples of strategies to improve the energy conversion performance. The working temperatures are $\hat{t}_- = 0.75$ and $\hat{t}_+ = 1.5$.

as magnetization and electric polarization, is strongly affected by the Clausius-Clapeyron coefficient which is a dimensionless parameter related to the change of the ferroic property across and the latent heat absorbed/emitted during the phase transformation. The average power output of cyclic phase transformation is studied based on two modes of heat exchange: i) alternating convective heating and cooling, and ii) continuous convective cooling and periodic radiative heating. Cycles optimized for the maximum power output are found.

We study in-depth a particular design of energy conversion devices using a material that undergoes antiferromagnetic to ferromagnetic phase transformation and the Faraday induction. We identify a dimensionless parameter called *the figure of merit* that influences significantly the efficiency and power output of energy conversion devices. The larger the figure of merit is, the higher the efficiency is. This parameter consists of material constants and design parameters, and is useful in material search and device design. Among other features, the dependence of the figure of merit on the shape of the working specimen is explored in detail. Two kinds of configurations are discussed. For one of them, thin film is proven to be the best geometry, while for the other, an optimized aspect ratio is found. In either case, such a dependence is weak, *i.e.* we will not be able to improve the performance too drastically by tuning the aspect ratio of the specimen.

Then, we combine our studies on cycles working at maximum power output and the performance analysis of the proposed energy conversion devices. We discussed the so-called design-task matching problem. The idea is that under a given working condition, *i.e.* the radiation power or the temperatures of heat reservoirs, there are only some particular devices, characterized by their figures of merit, that can perform the predicted maximum-power cycles. We call them the most suitable devices for the given working conditions. Similarly, we can define the best working conditions for the available devices. The results of this matching problem can be used to guide the choice of materials and the optimization of devices for the new energy conversion method.

Finally, by studying the performance based on the real material $Ni_{44}Co_6Mn_{40}Sn_{10}$, we realize that major improvements are required to make a device with the figure of merit in the order of 1. This could be done by material development or device design. On the side of material development, lowering the latent heat can significantly improve the performance, at least within the small z regime. On the side of device design, distributing a single load to a large number of small energy conversion units is another possible strategy to increase the figure of merit a lot.

Acknowledgments

This work is a part of the Ph.D. dissertation of YS, and supported by a Doctoral Dissertation Fellowship provided by the Graduate School of the University of Minnesota. YS also appreciates Richard D. James for encouraging and inspiring discussions during the preparation of this work.

References

1 W. Warburg, *Ann. Phys. (Leipzig)*, 1881, **13**, 141.
2 N. Tesla, *Pyromagneto-electric generator*, 1890, US Patent 428,057.
3 P. P. Kobeko and I. V. Kurchatov, *Z. Phys.*, 1930, **66**, 192.
4 E. Hegenbarth, *Cryogenics*, 1961, **1**, 242–243.
5 J. F. Scott, *Annu. Rev. Mater. Res.*, 2011, **41**, 229–240.
6 W. H. Clingman and R. G. Moore Jr., *J. Appl. Phys.*, 1961, **32**, 675.
7 J. D. Childress, *J. Appl. Phys.*, 1962, **33**, 1793–1798.
8 S. R. Hunter, N. V. Lavrik, T. Bannuru, S. Mostafa, S. Rajic and P. G. Datskos, SPIE Defense, Security, and Sensing, 2011, pp. 80350V–80350V.
9 V. K. Pecharsky and K. A. Gschneidner Jr., *Phys. Rev. Lett.*, 1997, **78**, 4497–4497.
10 A. S. Mischenko, Q. Zhang, J. F. Scott, R. W. Whatmore and N. D. Mathur, *Science*, 2006, **311**, 1270–1271.

11 V. Srivastava, Y. Song, K. Bhatti and R. D. James, *Adv. Energy Mater.*, 2011, **1**, 97–104.

12 K. A. Gschneidner Jr. and V. K. Pecharsky, *Annu. Rev. Mater. Sci.*, 2000, **30**, 387–429.

13 E. Brück, O. Tegus, D. C. Thanh and K. Buschow, *J. Magn. Magn. Mater.*, 2007, **310**, 2793–2799.

14 S. Fähler, U. K. Rößler, O. Kastner, J. Eckert, G. Eggeler, H. Emmerich, P. Entel, S. Müller, E. Quandt and K. Albe, *Adv. Eng. Mater.*, 2012, **14**, 10–19.

15 M. Valant, *Prog. Mater Sci.*, 2012, **57**, 980–1009.

16 J. R. Gómez, R. F. Garcia, A. D. M. Catoira and M. R. Gómez, *Renewable Sustainable Energy Rev.*, 2013, **17**, 74 – 82.

17 V. Srivastava, X. Chen and R. D. James, *Appl. Phys. Lett.*, 2010, **97**, 014101.

18 J. Liu, T. Gottschall, K. P. Skokov, J. D. Moore and O. Gutfleisch, *Nature Mater.*, 2012, **11**, 620–626.

19 J. Cui, Y. Wu, J. Muehlbauer, Y. Hwang, R. Radermacher, S. Fackler, M. Wuttig and I. Takeuchi, *Appl. Phys. Lett.*, 2012, **101**, 073904–073904.

20 W. S. Ginell, J. L. McNichols Jr. and J. S. Cory, *Mech. Eng.*, 1979, **101**, 28–33.

21 Y. Song, K. Bhatti, V. Srivastava, C. Leighton and R. D. James, *Energy Environ. Sci.*, 2013, **6**, 1315 – 1327.

22 V. K. Pecharsky, K. A. Gschneidner Jr, A. O. Pecharsky and A. M. Tishin, *Phys. Rev. B*, 2001, **64**, 144406.

23 F. L. Curzon and B. Ahlborn, *Am. J. Phys.*, 1975, **43**, 22.

24 P. Chambadal, *Les Centrales Nuclaires*, Armand Colin, Paris, 1957.

25 I. I. Novikov, *J. Nucl. Eng.*, 1958, **7**, 125–128.

26 M. Rubin, *Phys. Rev. A*, 1979, **19**, 1272–1276.

27 A. de Vos, *Endoreversible thermodynamics of solar energy conversion*, Oxford University Press, Oxford and New York, 1992.

28 K. H. Hoffmann, J. M. Burzler and S. Schubert, *J. Non-Equil. Thermodyn.*, 1997, **22**, 311–355.

29 C. Van den Broeck, *Phys. Rev. Lett.*, 2005, **95**, 2–4.

30 M. Esposito, K. Lindenberg and C. Van den Broeck, *Phys. Rev. Lett.*, 2009, **102**, 1–4.

31 R. S. Berry, V. A. Kazakov, S. Sieniutycz, Z. Szwast and A. M. Tsirlin, *Thermodynamics Optimization of Finite-Time Processes*, Wiley, Chichester, 2000.

32 K. H. Hoffmann, J. Burzler, A. Fischer, M. Schaller and S. Schubert, *J. Non-Equil. Thermodyn.*, 2003, **28**, 233–268.

33 H. Yan and H. Guo, *Phys. Rev. E*, 2012, **85**, 5–9.

34 V. Provenzano, A. J. Shapiro and R. D. Shull, *Nature*, 2004, **429**, 853–857.

35 R. Zarnetta, R. Takahashi, M. L. Young, A. Savan, Y. Furuya, S. Thienhaus, B. Maaß, M. Rahim, J. Frenzel, H. Brunken, Y. S. Chu, V. Srivastava, R. D. James, I. Takeuchi, G. Eggeler and A. Ludwig, *Adv. Funct. Mater.*, 2010, **20**, 1917–1923.

36 J. M. Ball and R. D. James, *Arch. Ration. Mech. Anal.*, 1987, **100**, 13–52.

37 K. Bhattacharya, *Microstructure of martensite : why it forms and how it gives rise to the shape-memory effect*, Oxford University Press, Oxford, 2003.

38 Z. Zhang, R. D. James and S. Müller, *Acta Mater.*, 2009, **57**, 4332–4352.

39 R. Delville, S. Kasinathan, Z. Zhang, J. V. Humbeeck, R. D. James and D. Schryvers, *Phil. Mag.*, 2010, **90**, 177–195.

40 J. Cui, Y. S. Chu, O. O. Famodu, Y. Furuya, J. Hattrick-Simpers, R. D. James, A. Ludwig, S. Thienhaus, M. Wuttig, Z. Zhang and I. Takeuchi, *Nature Mater.*, 2006, **5**, 286–290.

41 Y. Song, X. Chen, V. Dabade, T. W. Shield and R. D. James, *Nature*, 2013, **502**, 85–88.

42 A. G. Khachaturyan, S. M. Shapiro and S. Semenovskaya, *Phys. Rev. B*, 1991, **43**, 10832.

43 Y. M. Jin, Y. U. Wang, A. G. Khachaturyan, J. F. Li and D. Viehland, *Phys. Rev. Lett.*, 2003, **91**, 197601.

44 S. Kaufmann, U. K. Rößler, O. Heczko, M. Wuttig, J. Buschbeck, L. Schultz and S. Fähler, *Phys. Rev. Lett.*, 2010, **104**, 145702.

45 J. W. Gibbs, *Trans. Connecticut Academy Art Sci.*, 1873, **2**, 382–404.

46 S. Carnot, *Réflexions sur la puissance motrice du feu et sur les machines propres à développer cette puissance*, Bachelier, Paris, 1824.

47 K. P. Bhatti, S. El-Khatib, V. Srivastava, R. D. James and C. Leighton, *Phys. Rev. B*, 2012, **85**, 134450.

48 B. D. Culity and C. D. Graham, *Introduction to Magnetic Materials*, John Wiley & Sons, Inc., Hoboken, New Jersey, 2nd edn, 2009.

49 F. Terman, *Radio Engineers' Handbook*, McGraw-Hill, New York, 1943.

50 L. Lorenz, *Ann. Phys.*, 1879, **VII**, 161 – 193.

51 G. J. Snyder and T. S. Ursell, *Phys. Rev. Lett.*, 2003, **91**, 148301.

52 G. J. Snyder and E. S. Toberer, *Nat. Mater.*, 2008, **7**, 105–14.

53 S. S. Kutateladze and V. M. Borishanskii, *A Concise Encyclopedia of Heat Transfer*, Pergamon Press, 1966.